NASA CR- 166816

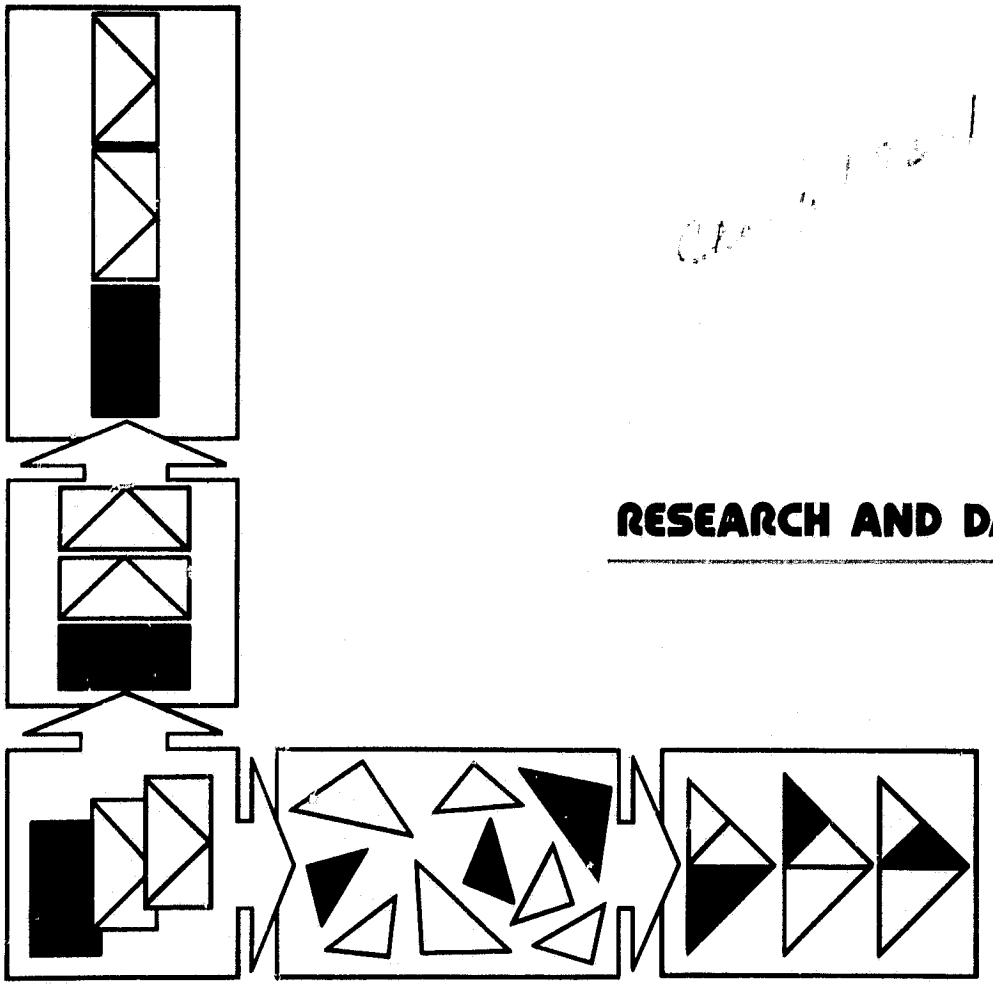

RESEARCH AND DATA SYSTEMS, INC.

DETERMINATION OF SEA SURFACE TEMPERATURES FROM MICROWAVE AND IR DATA

FINAL REPORT ON CONTRACT
NAS 5-26179

By

S. RANGASWAMY
and
JAMES GROVER

RESEARCH AND DATA SYSTEMS, INC.
9420 ANNAPOLIS ROAD
LANHAM, MARYLAND 20706

1.0 INTRODUCTION

Knowledge of sea surface temperatures (SST's) is extremely useful in many applications including commercial fishing, weather prediction and military uses. In the last two decades SST's have been determined from satellite-based radiometers by a number of authors including Fritz and Winston (1962), Smith et al (1970), Prabhakara and Dalu (1974), McClain and Abel (1977) and McClain (1980). Until recently, thermal infrared measurements in the 10.5 - 12.5 μm window region were mainly used for deriving SST's. In this spectral region the ocean surface behaves like an almost perfect blackbody radiator. The emissivity of the ocean has been estimated to be in the range of .967 to .997. By assuming it to be unity one can invert the Planck equation and compute SST.

Two basic problems limit the accuracy of SST's derived from thermal IR measurements. One is the presence of clouds in the field of view (FOV). Clouds, being at higher altitudes than the ocean surface, absorb the radiation from the ocean surface and reemit radiation corresponding to lower temperatures. Because of this even a small fractional coverage of the FOV will lead to unacceptable errors in the SST. It is, therefore, necessary to eliminate cloud-contaminated FOV's from SST computations.

The other problem limiting the accuracy of SST computations is the effect of the atmospheric constituents on the radiation emitted by the ocean. The atmosphere attenuates the radiation so that T_S, the sea surface temperature, is related to T_A, the equivalent temperature at the top of the atmosphere, by

$$T_S = T_A + \Delta T \qquad (1)$$

where ΔT is a correction term due to the atmosphere. This correction term is dependent mainly on atmospheric water vapor and could be greater than 8K in the tropical and subtropical areas. Currently a regression procedure is used in the NOAA operational SST production scheme GOSSTCOMP which uses the 10.5 - 11.5 μm measurements from the Advanced Very High Resolution Infrared Radiometer (AVHRR) on the TIROS-N series of NOAA satellites and the water vapor information from the High Resolution Infrared Sounder (HIRS) for the atmospheric correction (Walton, et al., 1976). This technique of finding the atmospheric correction has the drawback that the HIRS data provides relatively crude estimates

of temperature and humidity profiles and has a coarse spatial resolution compared with the AVHRR spatial resolution (McClain, 1980).

It is, therefore, necessary to look into the possibility of obtaining the atmospheric correction to the SST's derived from the thermal IR measurements. Multispectral IR measurements have been proposed for obtaining this correction by Anding and Kauth (1970), McMillin (1975), and Prabhakara et al (1974). In the present study a new method of obtaining the atmospheric correction is examined.

Microwave measurements from the Scanning Multichannel Microwave Radiometer (SMMR) on board the Nimbus-7 satellite are used to derive the precipitable water which is then used to obtain the atmospheric correction for use with AVHRR thermal IR measurements to obtain SST's. The microwave measurements are minimally affected by the presence of clouds so that they provide all-weather capability for the determination of SST and precipitable water. Thus the atmospheric correction, although at a relatively coarse resolution, is available over cloudy as well as cloud free areas. In this study, SST's derived from SMMR measurements are compared with SST's derived from both AVHRR and SMMR measurements, as well as with the operational AVHRR SST data.

2.0 COMPUTATION OF ATMOSPHERIC CORRECTION

2.1 Atmospheric Effects

As mentioned before, the temperatures observed by a satellite-based sensor are generally lower than the true surface temperature due to absorption and reemission by the atmosphere of the surface radiation. The atmsopheric constituents causing this attenuation are mainly carbon dioxide, ozone, water vapor and aerosols. Experimental measurements by Burch (1970) show that in the window region absorption by CO_2 is negligible. The same is true for ozone also. For the 10.5 μm to 12.5 μm region absorption and reemission by water vapor greatly exceed that by any other species except under very dry and hazy conditions (Bignell et al, 1963). The total water vapor absorption coefficient in the 10.5 μm - 12.5 μm region can be written as (Prabhakara et al, 1974)

$$K = K_e(\nu, T) + K_p(\nu, T) + K_l(\nu, T) \qquad (2)$$

where K_e and K_p are associated with the water vapor continuum and K_l with the water vapor lines. Experimental measurements by Burch (1970) and Bignell (1970) show that water vapor absorption depends strongly on the partial pressure of water vapor. Burch and Bignell have given the temperature variation of the mass absorption coefficients for water vapor. Their data can be used to compute the absorption by numerical integration of the equation of radiative transfer. This will enable us to compute the radiance transmitted from the bottom to the top of the atmosphere. We can then define the atmospheric correction ΔT as the difference between the surface temperature T_S and the equivalent temperature T_A at the top of the atmosphere for a given slant path through a cloud-free atmosphere.

2.2 Equation of Transfer

The basic equation of radiative transfer for an atmosphere in local thermodynamic equilibrium is

$$\frac{dI_\nu}{K_\nu \rho\, ds} = I_\nu - B_\nu(T) \qquad (3)$$

where I_ν is the radiant energy in the frequency interval $(\nu, \nu + d\nu)$, $K\nu$ is the absorption coefficient, ρ is the density, s the distance variable and B the Planck function. The formal solution of equation (3) is (Chandrasekhar, 1960)

$$I_S = I_O\, e^{-\tau(s,o)} + \int_o^s B(s,T)\, e^{-\tau(s,s')}\, R_\rho\, ds \qquad (4)$$

where $\tau(s,s')$ is the optical thickness of the material between the points s and s' given by

$$\tau(s,s') = \int_{s'}^{s} K_\rho ds \qquad (5)$$

By using equation (5) and defining $dm = \rho ds$ the general solution to the equation of radiative transfer becomes

$$I = I_O \exp\left(-\int_{m=o}^{M} k(m)\, dm\right) + \int_{m=o}^{M} k(m)\, B(m) \exp\left(-\int_{m=o}^{M} k(m')\, dm'\right) dm \qquad (6)$$

m is the water vapor mass along the path.

Following Cogan et al (1974) the atmosphere may be assumed to be made up of sufficiently thin layers in which variations are linear. Then

$$I_n = I_{n-1} \exp(-k_n M_n) + B(1 - \exp(-k_n M_n)) \qquad (7)$$

where M_n is the water vapor mass in a column of unit cross section in the layer n. k is the mass absorption coefficient in the 11.5 μm window (Bignell, 1970) consisting of two parts k_1 and k_2. k_1 is modified by changes in atmospheric pressure P from a standard value of 1000 mb, and k_2 is altered by changes in partial pressure e of water vapor from the standard value. k for the n^{th} layer may be written

$$k_n = k_1 \frac{Pn}{1000} + k_2 \frac{e_n}{1000} \qquad (8)$$

Bignell (1970) found that absorption by foreign broadening of water vapor lines (with coefficient k_1) has a positive temperature dependence of about 0.5% per °C and the e-type absorption (with coefficient k_2) has a strong negative dependence of about 2% per °C. Hence equation (8) can be written as

$$k_n = f_1(T)\, k_1 \left(\frac{Pn}{1000}\right) + f_2(T)\, k_2 \left(\frac{e_n}{1000}\right) \qquad (9)$$

where $f_1(T) = 1 - .005\,(303 - T_n)$ (10)

and $f_2(T) = 1 + .02\,(303 - T_n)$ (11)

T_n is the mean temperature in the nth layer.

2.3 Computation of Water Vapor Correction For The Thermal Window Channel

It is possible to compute the radiance observed by a satellite-based sensor at the top of the atmosphere from equation (7) provided temperature and water vapor pressure are available as a function of atmospheric pressure from the ocean to the top of the atmosphere. From this radiance the equivalent blackbody temperature at the top of the atmosphere, T_A (equation 1) can be obtained by inverting the Planck equation. The correction T is then given by the difference between the surface temperature T_s and the temperature at the top of the atmosphere T_A.

In this study, the total atmospheric water vapor obtained from SMMR measurements are used for predicting the atmospheric correction ΔT. Temperature and water vapor profiles are not available to evaluate this correction. Hence, it is necessary to determine the functional relationship between the correction ΔT and the total atmospheric water vapor W. Such a relationship can be obtained if a set of representative profiles of temperature and water vapor are available to compute both ΔT and W. For this study, due to the limited resources available, it was decided to use radiosonde data from ship soundings. These soundings were available on five tapes and covered the period February 11, 1979 through March 17, 1979. Altogether there were 91 useable soundings covering a wide range of latitudes and longitudes. These profiles were used to compute both T and W for a number of slant angles, 0, by using equations (7 and 1). The 91 sets of ΔT and W, as well as the temperature for the lowest point of the profile T_e were then input to a multiple regression routine which was used to determine the coefficients for a number of functional models. Eventually the following model was chosen on the basis of the multiple correlation coefficient and the sum of the squares of the residuals.

$$\Delta T = a_0 + a_1 \cdot W + a_2 \cdot W^2 + a_3 W \sec\theta + a_4 \cdot W \cdot \sec^2\theta + a_5 T_e \quad (12)$$

The multiple correlation coefficient for this equation was found to be .98. The various coefficients in this equation and their standard deviations are given in Table I T_e in equation (12) is considered to be quite close to the surface temperature T_s.

It is now possible to compute the atmospheric correction ΔT, given the precipitable water W and surface temperature T_s.

TABLE I

COEFFICIENTS OF EQUATION (12) AND THEIR STANDARD DEVIATIONS

Coefficients:	a_0	a_1	a_2	a_3	a_4	a_5
Value:	-4.315	0.8666	0.05648	-0.2718	-0.01603	0.01582
σ :	0.440	0.0940	0.00344	0.1216	0.04036	0.00130

3.0 COMPUTATION OF SEA SURFACE TEMPERATURES FROM AVHRR AND SMMR MEASUREMENTS

3.1 AVHRR Data

The Advanced Very High Resolution Radiometer (AVHRR) is a cross-track scanning radiometer with the spectral channels shown in Table II. The IFOV of the sensor is approximately 1.0 km at the sub-satellite point. For this study the Global Area Coverage (GAC) data at the reduced resolution of 4 km was used. This data was used in two forms. The first was the raw GAC 4 km data, from which, for each pixel, the latitude, longitude, solar zenith angle, angle of observation through the atmosphere, brightnesses from the visible channels, and the uncorrected 11 micron IR temperature can be figured. The temperature corrections are done starting with this IR data.

The other form is that of the operational NOAA GOSSTCOMP SST data derived from the AVHRR and HIRS data. This SST data, which is retrieved from observations averaged over 50 km target areas and stored on tapes covering seven day periods, is used in this study only for comparison with the corrected temperatures obtained from the raw AVHRR data.

3.2 SMMR Data

The Scanning Multichannel Microwave Radiometer (SMMR) (Figure 1) provides orthogonally polarized antenna temperature measurements at five microwave frequencies, 6.6 GHz, 10.7 GHz, 18.0 GHz, 21.0 GHz and 37.0 GHz with an absolute accuracy of less than 2°K (rms) at each frequency. The antenna's main beam is offset 42° from nadir and scans the earth in a conical pattern with a half angle of about 25° (Figure 2). The SMMR data used for this study was from SMMR CELL-ALL tapes, a product of the second stage of SMMR processing. Each logical record contains earth-located SMMR brightness temperatures for a block 780 km by 780 km on the surface of the earth. The antenna temperature measurements from the SMMR are converted to brightness temperatures and averaged into grids of various sizes based on the frequency of the observation. Table III shows the grid size, the number of bands and cells in each grid, and the frequencies of the observations which apply for each grid.

The SMMR brightness temperature for each cell of the 780 km x 780 km block have been corrected for the effects of the antenna sidelobe pattern. In addition the CELL-ALL tape brightness temperatures have been corrected for the

TABLE II

THE AVHRR CHANNEL SPECTRAL RANGES

CHANNEL	SPECTRAL RANGE	REGION
1	0.55 - 0.68	Visible
2	0.725 - 1.10	Visible/Near Infrared
3	3.55 - 3.93	Infrared
4	10.50 - 11.50	Infrared

SMMR INSTRUMENT CONFIGURATION

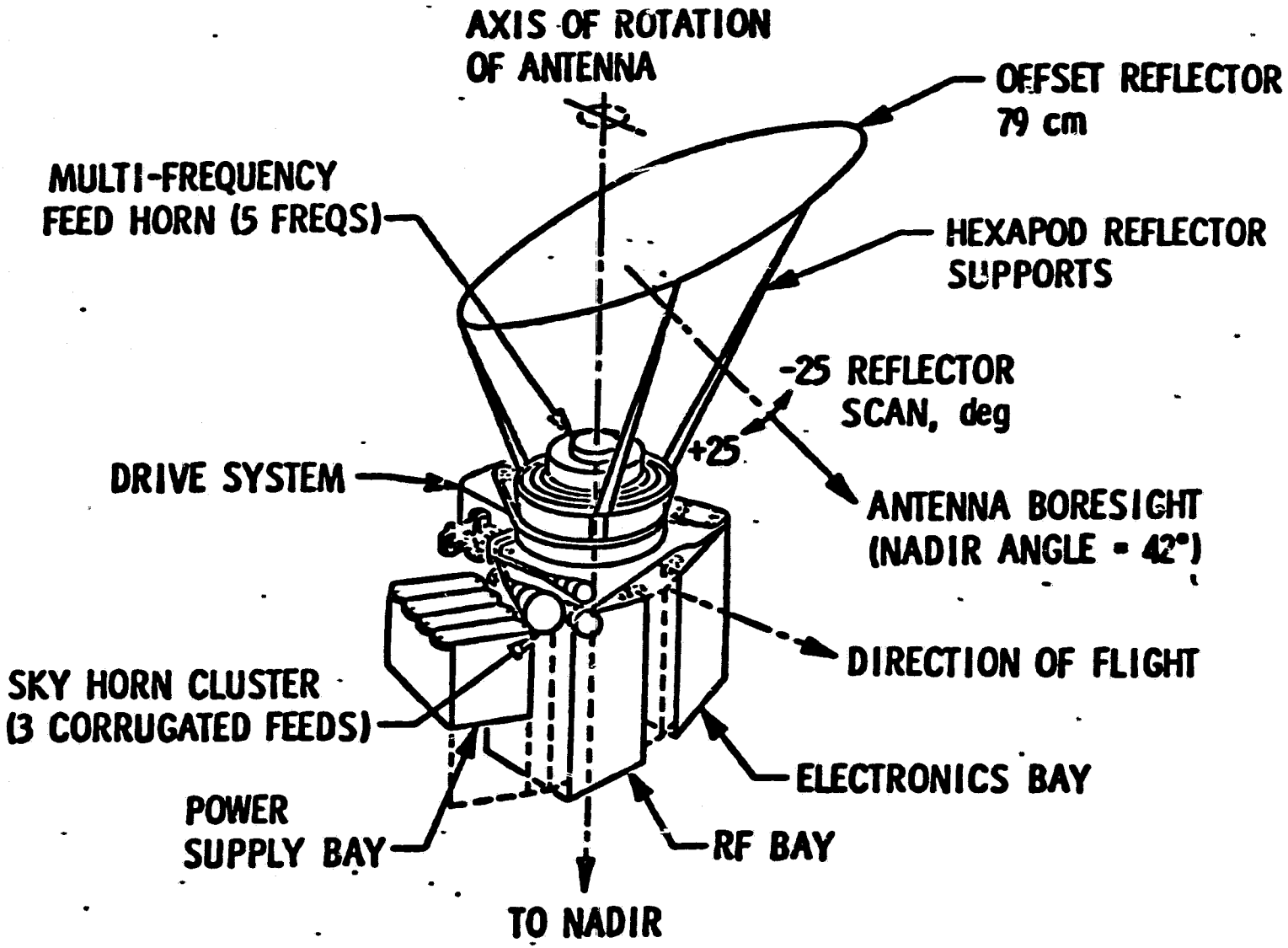

Figure 1

NIMBUS-G
SMMR SCAN GEOMETRY

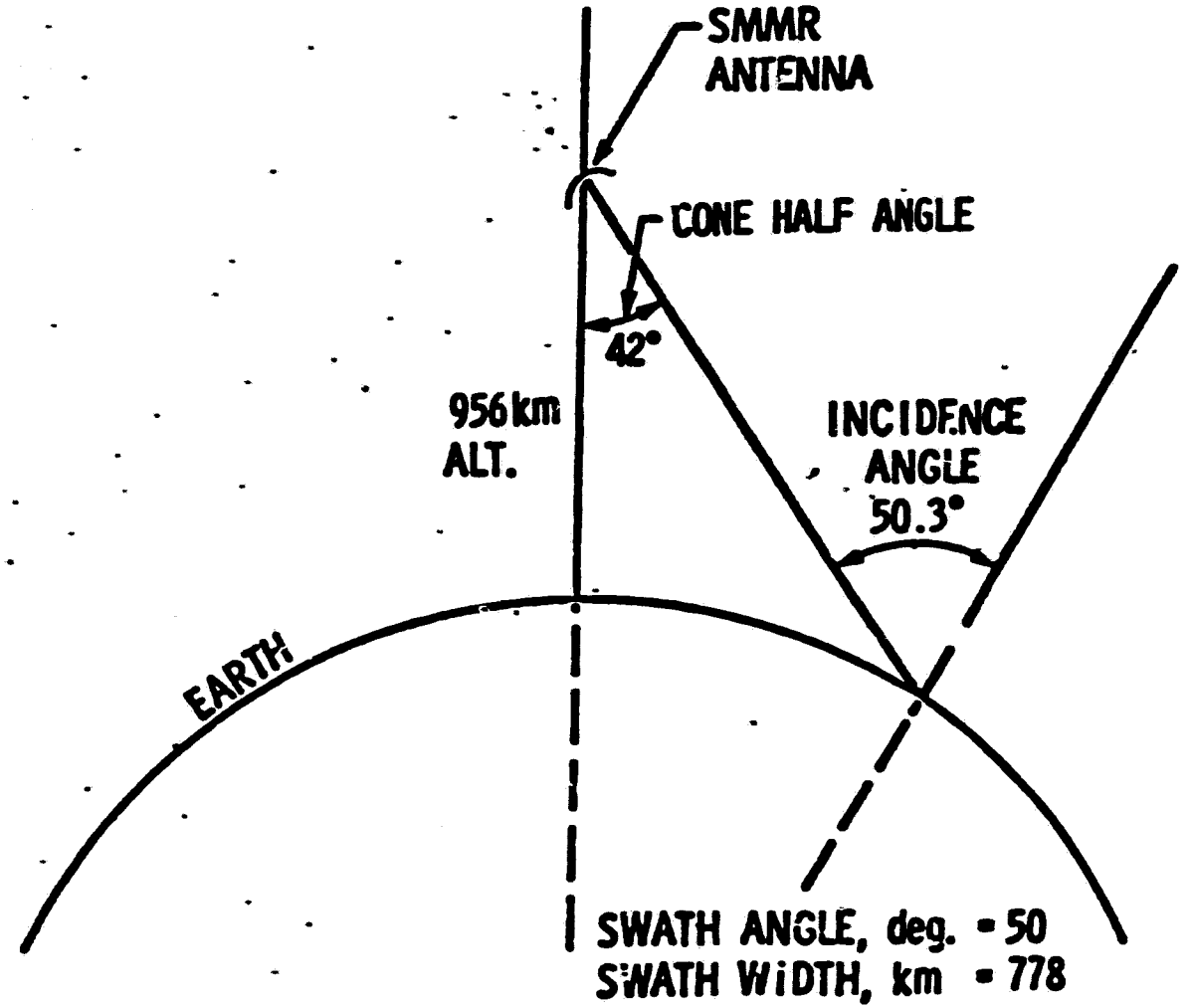

Figure 2

TABLE III

FREQUENCY AND CELL SIZE OF OBSERVATIONS ON THE SMMR CELL-ALL TAPE

GRID	GRID SIZE (km)	BANDS X CELLS	CHANNELS INCLUDED IN GRID (GHz)
1	156.0	5 x 5	37.0, 21.0, 18.0, 10.7, 6.6
2	97.5	8 x 8	37.0, 21.0, 18.0, 10.7
3	60.0	13 x 13	37.0, 21.0, 18.0
4	30.0	26 x 26	37.0

effects of polarization mixing between the vertically and horizontally polarized components of the signal received by the SMMR antenna.

To retrieve atmospheric water vapor and (SMMR) sea surface temperatures, the algorithms developed by Wilheit and Chang (1980) may be used on the cell data. The water vapor algorithm uses the 37.0, 21.0 and 18.0 GHz channel information, which is available for the 13 x 13 grid whose cell size is 60.0 km on each side as well as for coarser grids, while the SST algorithm uses information from all channels, which is only available from the 5 x 5 156.0 km square grid. The 13 x 13 60 km SMMR grid was chosen as the reference grid, into which AVHRR pixels would be registered, and SMMR SST's interpolated.

Only data from the ascending (daytime) nodes of SMMR were used, so as to allow the closest time coincidence with the AVHRR ascending (daytime) data. The local time for an ascending SMMR node is always about noon (12:00 hours), and the local time for an ascending AVHRR node is always about 3 p.m. (15:00 hours). It was decided for this study that the resulting 3 hours difference is insignificant for 60 km square areas for those parameters measured by SMMR.

3.3 Overview of Computation of SST's

Figure 3 gives a gross schematic of the computation of SST's by using both AVHRR and SMMR data. First, total atmospheric water vapor W is computed from SMMR brightness temperatures. The precipitable water is then used to compute atmospheric correction as explained in Section 2.0. The correction uses the brightness temperature T_A for the 11.5 μm channel over clear areas from the AVHRR GAC data (Section 3.5 regarding cloud filtering). T_A has not been corrected for atmospheric effects. It is used as a first approximation for the surface temperature. The ΔT so derived is then used to correct T_A and obtain the first approximation of the corrected surface temperature T_s. This is again input into equation (12) and ΔT is computed a second time. This ΔT is then used to correct T_A again to obtain a final surface temperature (SST_A) from AVHRR brightness temperatures.

Sea surface temperatures are also computed from SMMR brightness temperatures directly by using the algorithm of Wilheit and Chang (1980) (Section 3.2). These are denoted by SST_S. Finally, the corresponding sea surface temperatures from the NOAA operational product SST_O are extracted from the seven day GOSSTCOMF tapes. The three sets of SST's are then compared and the statistics of the residuals are computed.

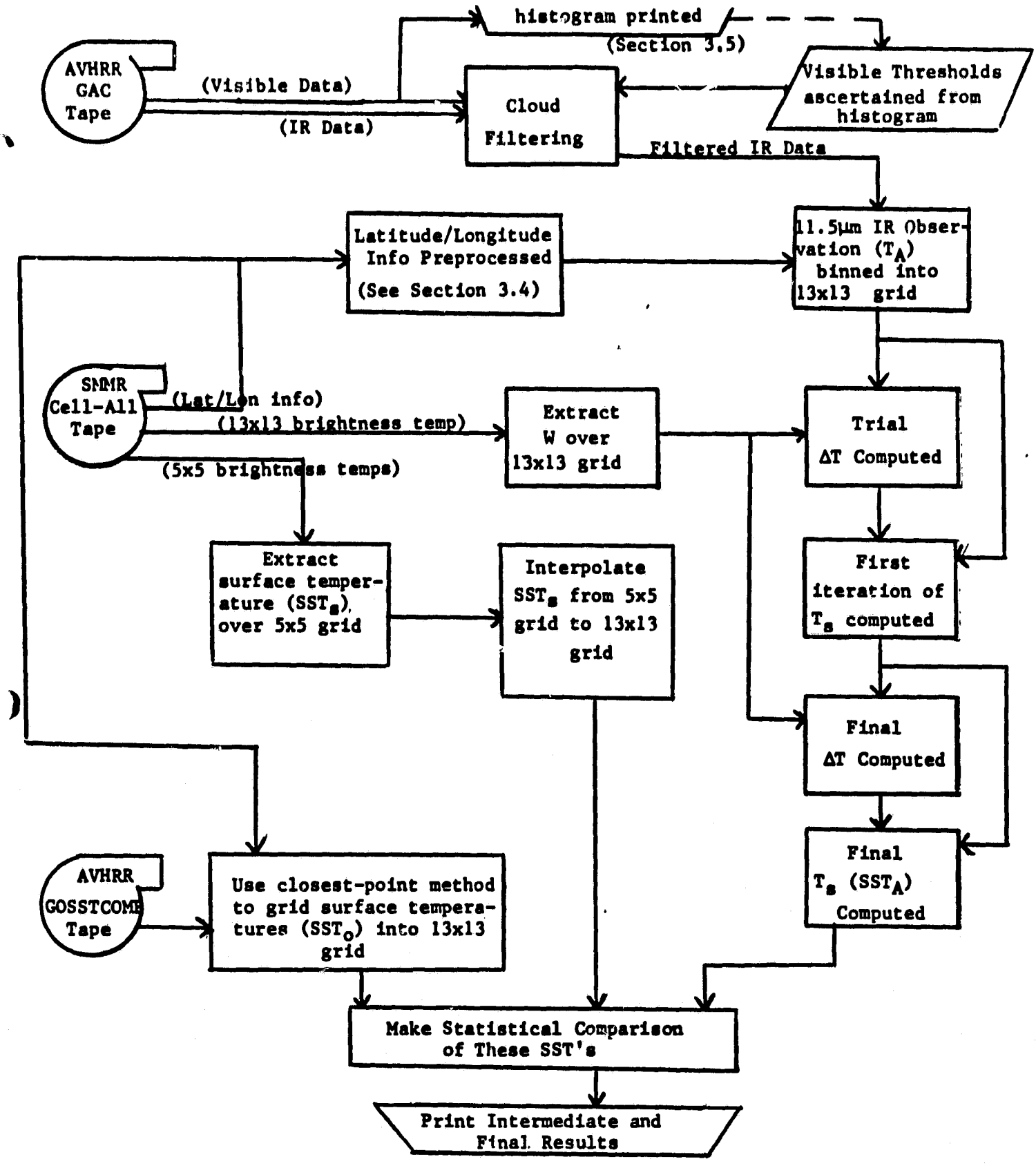

FIGURE 3

OVERALL SCHEMATIC OF COMPUTATIONS AND COMPARISONS OF SST's FROM AVHRR AND SMMR DATA

3.4 Area Selection and Data Handling

Six open ocean areas were initially selected, on the basis of the 20° x 20° open ocean blocks used in Kogut and Hopkins (1980). SMMR CELL-ALL data covering the time from February 15 to March 17, 1979 were used to plot the approximate locations of the centers of all 780 x 780 km SMMR blocks from each of the days covered by the tape.

AVHRR visible and infrared imagery was then used to ascertain, out of all the locations of SMMR blocks within the initially selected areas, which locations were relatively clear. A little patchy cloudiness was acceptable, so long as there were sufficient areas to ensure that at least isolated pixels of infrared data would reach from the surface over most of where the 780 x 780 km SMMR block covered. Visible and IR GOES prints were used to supplement this information where possible.

Based on this information, AVHRR GAC data was ordered for ten coverages of a region on the earth on a given day. After the selected-coverage GAC data arrived, both AVHRR visible histogram runs (see Section 3.5) and temperature estimation runs (following the algorithm of Section 3.3) were made. In each run, the SMMR tape was scanned first, until an ascending-node (daytime) block within the given region and day was found. An array representing a grid of latitude and longitude lines covering the 780 x 780 km SMMR block was then filled in with information about how far over and how far up on the SMMR block each grid point was. This was done by:

1. Figuring what the proper rotation and stretching algorithms would be, were the earth's surface flat, from the latitude/longitude grid to the mesh of 60 x 60 km cell centers in the SMMR block, based on the latitudes and/or longitudes of three cell centers.
2. For each cell, obtaining the residual between its true latitude/longitude and that computed from the inverse of the transformation from (1) above.
3. For each point in the latitude/longitude grid,
    (a) finding its supposed SMMR block position from the transformation of (1);

(b) using that position to interpolate what residual there would be from the inverse transformation from around that position to latitude and longitude; and

(c) adding that residual (calculated minus real latitude/longitude) to the latitude/longitude of the latitude/longitude grid point and obtaining (a reasonably) true SMMR block location by using the (forward) transformation of (1).

In temperature runs, the SMMR water vapor values were computed directly from the 60 x 60 km cell data, while the sea surface temperatures were computed from the 156 x 156 km cell data. A polynomial was then fitted over the SST's, and was then evaluated at the center of each 60 x 60 km cell.

The AVHRR tape file for the corresponding region was then read, and for each AVHRR pixel, the corresponding 60 x 60 km SMMR cell was found by interpolating the pixel's latitude and longitude on the grid for SMMR block location. In histogram runs, the visible values were used if the pixel was within the 780 x 780 km block at all. In temperature runs, the IR value was added in as part of an averaging process for every 60 x 60 km cell. For all runs, the final calculations and printouts were done after the AVHRR tape file had been completely read.

3.5 Cloud Filtering of AVHRR Data

The identification of cloudy pixels was done by establishing brightness thresholds for two of the visible "reflectance channels". The two channels used were the red (0.725-1.10 μm) and green (0.55-0.68 μm) of the AVHRR. The radiances in these channels were normalized by dividing by the cosine of the solar zenith angle.

Special runs were made to obtain histograms of the radiances in each channel, which were then plotted on the printer output. A typical pair of histograms are shown in Figures 4 and 5.

The large peak at the low radiance end of the histogram corresponds to reflection from the ocean surface. Peaks at higher radiances correspond to reflection from cloud-ocean combinations or from clouds. The cloud-no cloud threshold was selected to be $R_o + \Delta R$ where R_o is the radiance corresponding to

**********HISTOGRAM OF VIS-RED

0		LT	1.00	:	
0	1.00	TO	2.00	:	
0	2.00	TO	3.00	:	
48	3.00	TO	4.00	:	*
***	4.00	TO	5.00	:	************************************
***	5.00	TO	6.00	:	**
***	6.00	TO	7.00	:	**
***	7.00	TO	8.00	:	**
***	8.00	TO	9.00	:	**
947	9.00	TO	10.0	:	**********************************
646	10.0	TO	11.0	:	**************************
532	11.0	TO	12.0	:	**********************
420	12.0	TO	13.0	:	******************
335	13.0	TO	14.0	:	**************
334	14.0	TO	15.0	:	**************
275	15.0	TO	16.0	:	************
249	16.0	TO	17.0	:	**********
224	17.0	TO	18.0	:	*********
222	18.0	TO	19.0	:	*********
168	19.0	TO	20.0	:	******
172	20.0	TO	21.0	:	*******
154	21.0	TO	22.0	:	******
138	22.0	TO	23.0	:	*****
137	23.0	TO	24.0	:	*****
141	24.0	TO	25.0	:	*****
143	25.0	TO	26.0	:	*****
125	26.0	TO	27.0	:	*****
126	27.0	TO	28.0	:	*****
111	28.0	TO	29.0	:	****
121	29.0	TO	30.0	:	****
112	30.0	TO	31.0	:	****
112	31.0	TO	32.0	:	****
99	32.0	TO	33.0	:	****
113	33.0	TO	34.0	:	****
94	34.0	TO	35.0	:	***
100	35.0	TO	36.0	:	****
94	36.0	TO	37.0	:	***
81	37.0	TO	38.0	:	***
90	38.0	TO	39.0	:	***
82	39.0	TO	40.0	:	***
95	40.0	TO	41.0	:	***
103	41.0	TO	42.0	:	****
69	42.0	TO	43.0	:	**
57	43.0	TO	44.0	:	**
62	44.0	TO	45.0	:	**
52	45.0	TO	46.0	:	**
60	46.0	TO	47.0	:	**
60	47.0	TO	48.0	:	**
51	48.0	TO	49.0	:	**
160		GT	49.0	:	******

FIGURE 4

TYPICAL HISTOGRAM OF THE RADIANCES IN THE RED (0.72-1.10 um) AVHRR CHANNEL

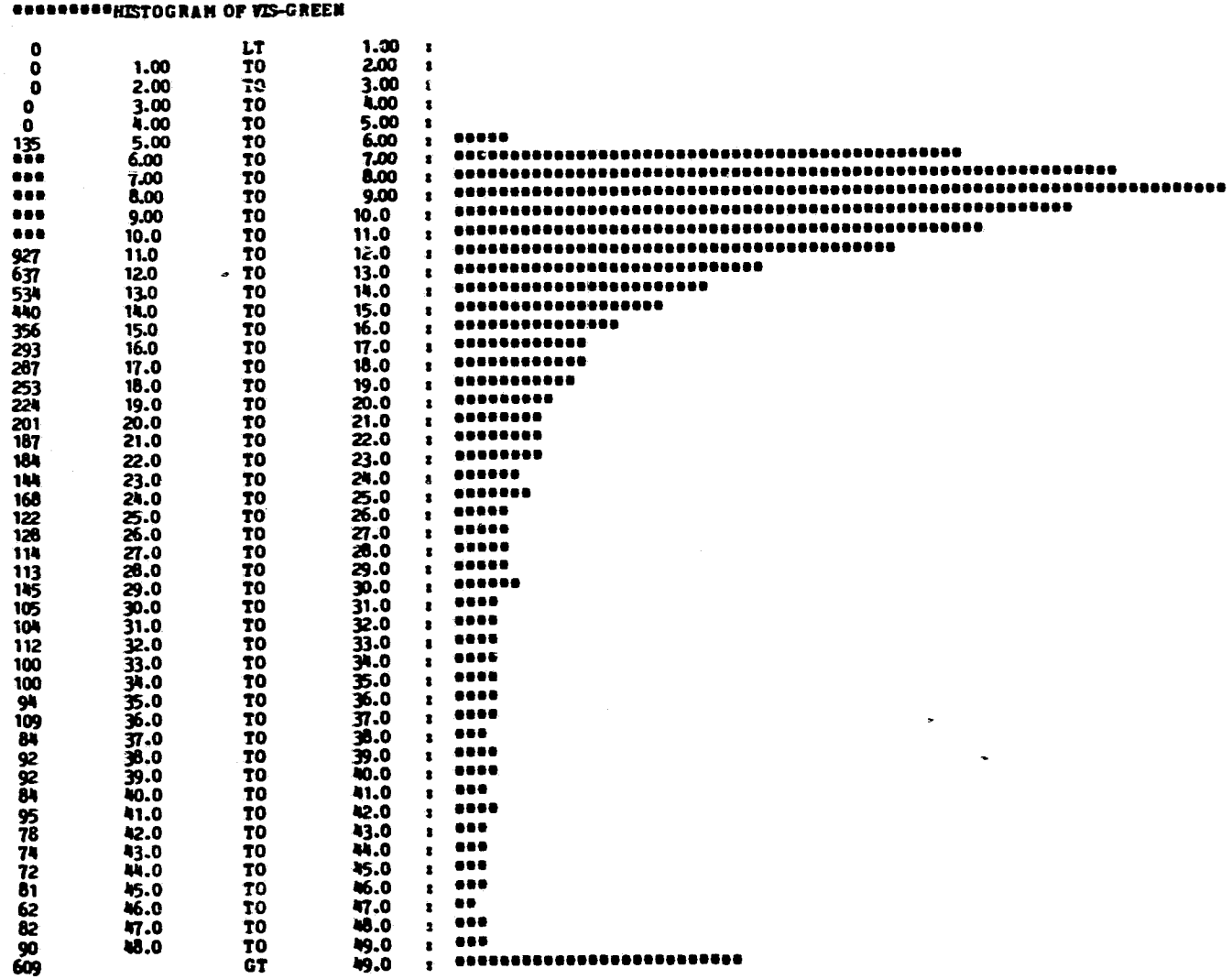

FIGURE 5

TYPICAL HISTOGRAM OF THE RADIANCES IN THE GREEN (0.55-0.68 um) AVHRR CHANNEL

the peak representing reflections from the ocean and ΔR is determined from the frequency distribution between this peak and the cutoff of the lower radiance half of the histogram. ΔR was chosen conservatively so as to preclude even small fractions of cloud coverage in the FOVs.

The threshold for each visible channel was then entered as input into the temperature runs, which would compare the normalized radiance from each channel for each AVHRR pixel with the corresponding threshold, and use the IR from the pixel only if each radiance was less than the corresponding threshold.

4.0 RESULTS

Seven SMMR blocks of 780 x 780 km have been used for analysis in this study (Figure 6). Tables IV(a) through IV(j) show some of the results for the block centered at 279.9°S latitude, 18.9°W longitude, on February 27, 1979. The 13 x 13 elements of Tables IV(b) through IV(j) refer to the SMMR 60 x 60 km cells over which the average water vapor is retrieved. Table IV(a) shows the SST's retrieved from SMMR brightness temperature data over the 5 x 5 156 km grid. Table IV(b) shows the interpolation of this over the 13 x 13 60km grid. The temperatures seem to be very low for latitudes in the order of 28°S. Table IV(c) shows the total water vapor for each 60 km cell. The values range from 2.7 gm/cm^2 to 4.7 gm/cm^2. These water vapor values are available even for those pixels which are defined as cloudy by visible threshold. Table IV(d) shows how many AVHRR pixels were used for each 60 km cell. These numbers show where there are areas of partial cloudiness and complete overcast.

Table IV(e) shows the brightness temperature of the AVHRR thermal channel for each pixel. These values are, as yet, not corrected for atmospheric water vapor. They are on the order of 291°K. Table IV(f) shows the final corrected SST computed by adding the atmospheric correction derived from SMMR data to the brightness temperatures derived from AVHRR data. It may be observed from Table IV(f) that the SST values are on the order of 296°K, considerably higher than the SMMR derived SST's. Table IV(g) shows the SST's from the NOAA operational product tape which were gridded on the SMMR 60 km grid by the nearest neighbor approach. It may be seen from Table IV(g) that the values are close to the SST derived from AVHRR and SMMR. Tables IV(h) through IV(j) summarize residuals between different methods of deriving the SST, as follows:

Table IV(h):	SST(AVHRR & SMMR) - SMMR(AVHRR OPERATIONAL)
Table IV(i):	SST(AVHRR & SMMR) - SST(SMMR)
Table IV(j):	SST(SMMR) - SST(AVHRR OPERATIONAL)

It may be observed that the SST derived from AVHRR and SMMR is at most about a degree less, on the average, than the NOAA operational AVHRR, while the SMMR SST is about 21 or 22 degrees less than both of these. This, in combination with the latitude, would seem to indicate that the AVHRR-SMMR derived product corresponds at least reasonably well to surface truth, while the SMMR product is at

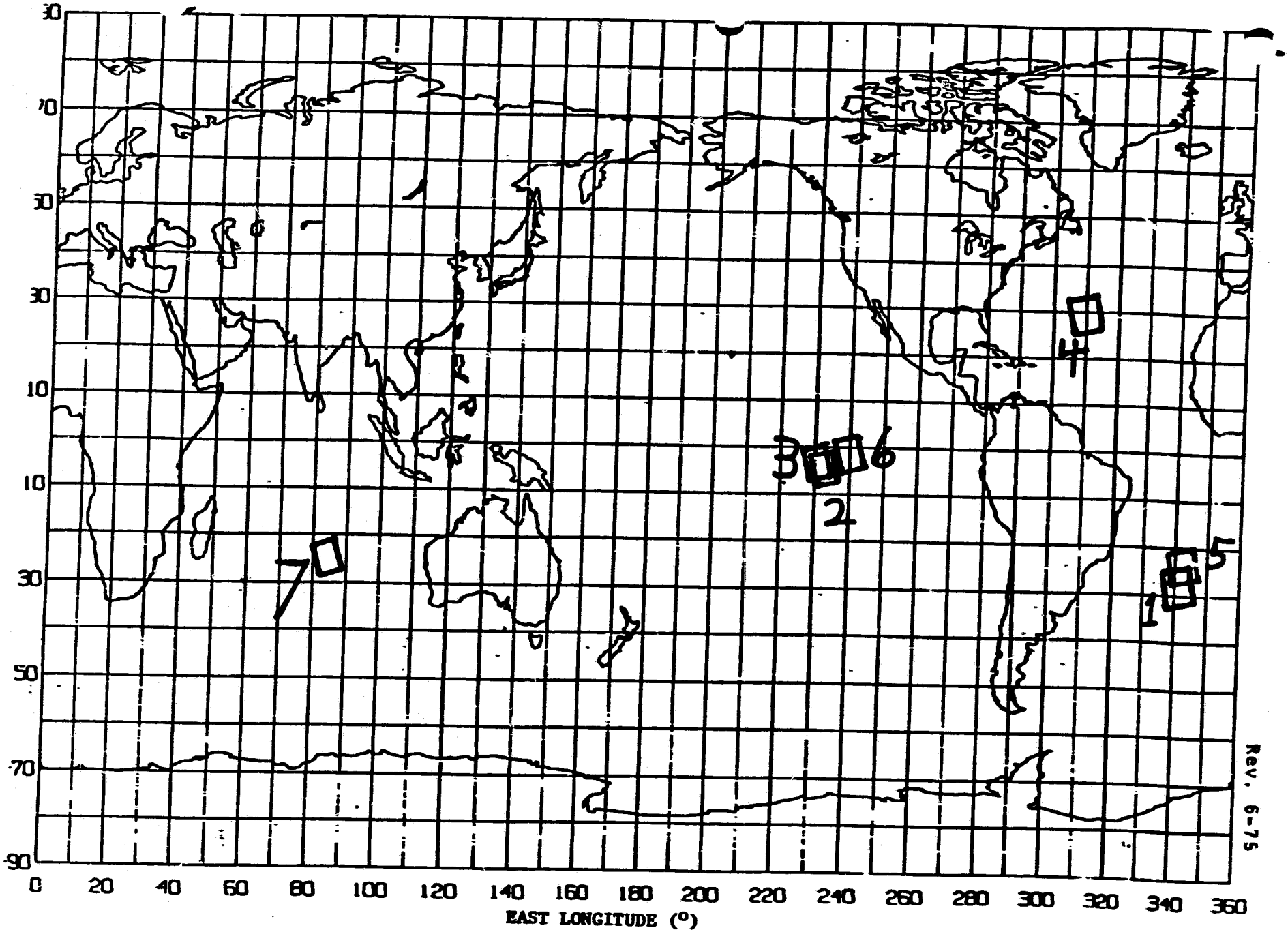

FIGURE 6.

LOCATIONS OF THE 780x780 SMMR BLOCKS USED FOR ANALYSIS

TABLE IV(a) SMMR SST's (°K) RETRIEVED OVER THE 5x5 GRID

273.12	276.57	274.29	277.37	278.47
274.26	275.64	275.10	277.56	278.98
274.26	273.34	276.95	275.35	277.64
274.56	274.15	275.14	275.13	277.45
274.07	273.55	273.69	274.31	275.23

TABLE IV(b) SMMR SST's (°K) INTERPOLATED OVER THE 13x13 GRID

SMMRSST (13.13): (AVERAGE = 272.44

273.5	273.7	274.0	274.3	274.7	275.1	275.6	276.1	276.7	277.4	278.1	278.8	279.6
273.8	274.0	274.2	274.6	274.8	275.2	275.7	276.2	276.7	277.4	278.0	278.7	279.5
274.0	274.2	274.4	274.6	274.9	275.3	275.7	276.2	276.7	277.3	277.9	278.6	279.4
274.2	274.3	274.5	274.7	275.0	275.3	275.7	276.2	276.7	277.2	277.8	278.5	279.2
274.3	274.4	274.6	274.8	275.0	275.3	275.7	276.1	276.6	277.1	277.6	278.2	278.9
274.4	274.5	274.6	274.8	275.0	275.2	275.6	275.9	276.4	276.9	277.4	278.0	278.6
274.5	274.5	274.6	274.7	274.9	275.1	275.4	275.8	276.2	276.6	277.1	277.7	278.3
274.5	274.5	274.5	274.6	274.7	275.0	275.2	275.5	275.9	276.3	276.8	277.3	277.9
274.4	274.4	274.4	274.4	274.6	274.7	275.0	275.2	275.6	276.0	276.4	276.9	277.5
274.3	274.2	274.2	274.2	274.3	274.5	274.7	274.9	275.2	275.6	276.0	276.5	277.0
274.1	274.0	274.0	274.0	274.0	274.1	274.3	274.5	274.8	275.1	275.5	275.9	276.4
273.9	273.8	273.7	273.7	273.7	273.8	273.9	274.1	274.3	274.6	275.0	275.4	275.8
273.7	272.5	272.4	272.2	272.3	272.4	273.5	273.6	273.8	274.1	274.4	274.8	275.2

TABLE IV(c) SMMR TOTAL WATER VAPOR (gm/cm^2) RETRIEVED OVER THE 13x13 (60 km) GRID

SMFWV (13.13) (AVERAGE = 3.3493

4.111	4.407	4.164	2.948	3.512	3.570	4.332	4.746	4.191	4.084	3.695	3.559	3.600
4.550	4.379	4.181	3.640	3.461	3.639	4.114	4.007	3.936	3.797	3.602	3.440	3.492
4.242	4.044	3.634	3.575	3.375	3.425	3.610	3.676	3.722	3.597	3.310	3.315	3.201
3.832	3.698	3.568	3.259	3.057	3.100	3.211	3.481	3.477	3.123	3.079	3.002	2.886
3.519	3.446	3.203	3.123	2.900	3.078	2.982	2.854	2.908	3.048	2.815	2.733	2.732
3.362	3.678	2.155	2.036	2.264	2.178	3.000	2.960	3.126	3.036	2.100	2.011	2.765
3.344	3.179	3.341	3.080	3.231	3.209	3.311	2.936	3126	3.224	3.162	3.064	2.874
3.497	3.361	3.340	3.239	3.259	3.021	3.279	3.171	3.054	2.984	2.981	2.857	2.696
3.607	3.301	3.348	3.349	3.236	3.003	3.267	3.260	3.172	3.240	3.183	3.007	3.096
3.798	3.512	3.442	3.147	3.279	3.283	3.185	3.326	3.130	3.088	3.286	3.350	3.196
3.750	3.566	3.451	3.421	3.842	3.469	3.454	3.420	3.124	3.046	2.993	3.109	3.223
3.443	3.374	3.314	3.322	3.404	3.854	3.273	3.237	3.340	3.034	3.004	3.167	3.202
3.227	3.217	3.130	3.217	3.286	3.285	3.193	3.034	3.360	3.135	2.981	2.948	2.993

TABLE IV(d) NUMBER OF AVHRR PIXELS USED IN EACH 60 KM CELL

0	0	4	5	0	0	0	1	0	0	3	5	2
0	0	24	35	0	0	0	0	0	3	3	50	12
0	7	42	55	7	0	0	0	6	40	24	11	3
18	37	64	76	52	15	7	9	46	53	17	7	22
48	71	39	74	48	85	39	42	83	89	53	15	40
34	10	46	49	28	72	44	39	47	25	42	59	57
26	37	65	39	27	55	47	9	8	15	15	39	70
46	41	54	40	27	21	46	27	84	98	53	129	131
74	47	38	46	67	56	38	73	71	94	86	38	76
80	43	52	63	81	83	77	93	65	4	30	25	14
68	47	37	58	82	58	98	107	76	0	3	11	50
65	65	58	71	50	72	84	85	89	34	52	110	52
50	66	57	34	83	69	90	73	109	110	123	76	101

TABLE IV(e) UNCORRECTED AVERAGE AVHRR BRIGHTNESS TEMPERATURE OVER EACH 60 KM CELL

GACIG (12.12) (AVERAGE = 191.50

.0	.0	290.9	290.9	.0	.0	.0	291.1	.0	.0	291.0	291.0	289.6
.0	.0	291.1	291.2	.0	.0	.0	.0	.0	292.2	292.5	292.3	291.0
.0	290.9	291.6	291.8	291.5	.0	.0	.0	291.5	292.5	292.8	292.5	291.1
290.3	291.5	292.3	293.1	292.4	291.3	291.1	291.5	291.8	292.7	293.1	292.9	292.9
290.8	291.7	291.9	292.8	292.8	292.7	292.6	293.0	293.4	293.6	293.8	293.4	293.4
291.2	291.6	292.7	293.0	291.6	292.6	292.6	292.6	292.8	293.3	293.7	293.7	293.5
291.6	291.6	292.1	291.7	291.0	292.2	292.1	291.5	291.7	292.4	292.5	292.9	293.5
291.3	290.8	291.8	292.6	291.2	291.6	291.9	292.0	292.5	293.0	293.6	293.4	293.7
291.3	291.0	290.9	291.3	292.0	291.3	291.4	291.8	292.3	292.7	292.7	293.3	292.6
291.2	290.5	291.0	291.2	292.0	291.8	291.5	291.6	291.6	291.5	292.0	291.5	291.7
290.5	290.4	291.4	290.9	291.6	291.8	291.8	292.0	291.8	.0	290.7	291.5	291.7
290.0	290.4	290.6	290.6	291.0	291.1	291.4	291.7	291.8	291.3	291.5	291.6	291.5
289.8	290.1	290.0	290.6	290.7	290.8	291.2	291.2	291.9	291.7	292.1	291.6	291.6

TABLE IV(f) FINAL CORRECTED SST's FROM SMMR AND AVHRR MEASUREMENTS

GCTMP2 (13.13): (AVERAGE = 296.16)

.0	.0	298.1	297.4	.0	.0	.0	298.6	.0	.0	295.5	294.3	293.7
.0	.0	298.4	296.6	.0	.0	.0	.0	.0	297.1	296.8	296.3	295.0
.0	297.9	297.9	297.3	296.3	.0	.0	.0	295.4	297.1	296.8	296.3	294.7
296.9	297.6	297.9	297.8	296.6	295.5	295.4	296.1	296.3	296.5	296.7	296.3	296.0
296.4	297.1	296.6	297.2	296.6	296.8	296.4	296.5	296.9	297.2	297.1	296.4	296.3
296.4	295.9	297.3	297.2	296.2	296.9	296.4	296.3	296.7	296.9	297.4	297.0	296.5
296.7	296.2	297.1	296.0	296.5	296.5	296.5	296.1	295.6	294.3	294.5	296.3	394.4
296.9	295.9	296.7	296.1	295.8	295.5	296.2	296.0	296.2	296.5	296.5	296.5	296.6
297.1	295.9	295.9	296.2	296.4	295.2	295.7	296.0	296.2	296.6	296.4	296.7	296.0
297.6	296.0	296.1	295.6	296.5	296.2	295.6	295.9	295.4	295.2	295.8	295.4	295.1
296.7	296.0	296.6	295.9	296.7	296.6	296.4	296.5	295.6	.0	294.1	295.0	295.1
295.4	295.4	295.4	295.3	295.8	296.4	295.7	295.8	295.9	294.8	294.5	296.1	295.1
294.5	294.8	294.4	296.1	296.2	295.2	295.3	294.9	296.0	295.4	295.4	294.8	294.8

TABLE IV(g) NOAA OPERATIONAL PRODUCT SST's INTERPOLATED OVER THE 13x13 GRID

AVHTMF (13.13) (AVERAGE = 197.00)

296.9	296.9	296.9	296.9	296.9	296.9	296.9	296.9	296.9	296.9	296.9	296.9	296.8
296.9	296.9	296.9	296.9	296.9	296.9	296.9	296.9	296.9	296.9	296.9	296.9	296.9
296.9	296.9	296.9	296.9	296.9	296.9	296.9	296.9	296.9	296.9	296.9	296.9	296.9
296.9	296.9	296.9	296.9	296.9	296.9	296.9	296.9	296.9	296.9	296.9	296.9	296.9
296.9	296.9	296.9	296.9	296.9	296.9	296.9	296.9	296.9	297.3	297.3	297.3	297.3
297.7	297.7	297.7	297.7	297.7	297.7	297.7	297.7	297.7	297.7	297.7	297.7	297.7
297.7	297.7	297.7	297.7	297.7	297.7	297.7	297.7	297.7	297.7	297.7	297.7	297.7
297.7	297.7	297.7	297.7	297.7	297.7	297.7	297.7	297.7	297.7	297.7	297.7	297.7
297.7	297.7	297.7	297.7	297.7	297.7	297.7	297.7	297.7	297.7	297.7	297.7	296.7
296.2	296.2	296.2	296.2	296.2	296.2	296.2	296.2	296.2	296.2	297.0	297.0	297.0
296.2	296.2	296.2	296.2	296.2	296.2	296.2	296.2	296.2	296.2	296.2	296.2	297.0
296.2	296.2	296.2	296.2	296.2	296.2	296.2	296.2	296.2	296.2	296.2	296.2	296.2
296.3	296.3	296.3	296.3	296.3	296.3	296.3	296.3	296.3	296.3	296.2	296.2	296.3

TABLE IV(h) RESIDUALS BETWEEN SST(AVHRR & SMMR) AND SST(AVHRR OPERATIONAL)

RSIDAC (13.13): (AVERAGE = -0.85433)

0.0	0.0	1.20	0.488	0.0	0.0	0.0	1.62	0.0	0.0	-1.40	-2.69	-3.14
0.0	0.0	1.42	-.327	0.0	0.0	0.0	0.0	0.0	0.123	-.110	-.643	-1.97
0.0	0.993	0.914	0.313	-.423	0.0	0.0	0.0	-.556	0.132	-.134	-.612	-2.29
-.603E-01	0.637	0.959	0.828	-.355	-1.45	-1.57	-.863	-.649	-.471	-.242	-.646	-.909
-.579	0.103	-.366	0.252	-.342	-.105	-.543	-.419	-.4882-01	-.113	-.294	-.905	-1.06
1.39	1.00	.428	.547	1.58	.632	1.32	1.44	1.89	.849	.272	.762	1.25
-1.07	-1.52	-.663	-1.75	-2.26	-1.20	-1.23	-2.61	-2.17	-1.47	-1.55	-1.41	-1.15
-.879	-1.86	-1.05	-1.64	-1.99	-2.25	-1.51	-1.72	-1.57	-1.28	-1.22	-1.21	-1.19
-.641	-1.87	-1.87	-1.59	-1.30	-2.56	-2.04	-1.76	-1.55	-1.10	-1.38	-.374	-.751
1.35	-.269	-.131	-.621	0.282	-.420E-01	-.608	-.375	-.865	-1.03	-1.24	01.68	-1.90
0.484	-.221	0.307	-.368	0.414	0.316	0.191	0.203	-.667	0.0	-2.19	-1.28	-1.91
-.884	-.810	-.811	-.931	-.458	-.822	0.578	0.476	-.341	-1.46	-1.35	-1.11	-1.16
-1.86	-1.58	-1.95	-1.28	-1.12	-1.14	-1.05	-1.40	-.311	-.969	-.955	-1.58	-1.54

RESIDUAL STATISTICS:
AVERAGE = -0.85433 MINIMUM = -3.1382 , MAXIMUM = 1.6172
STANDARD DEVIATION = 0.87417 : THE NUMBER OF OBSERVATIONS = 150.

TABLE IV(i) RESIDUALS BETWEEN SST(AVHRR & SMMR) AND SST(SMMR)

RSIDAS (13.13): AVERAGE = 20.691

0.0	0.0	24.2	23.1	0.0	0.0	0.0	22.4	0.0	0.0	17.6	15.5	14.1
0.0	0.0	24.2	22.1	0.0	0.0	0.0	0.0	0.0	19.7	18.8	17.6	15.5
0.0	23.8	23.5	22.6	21.4	0.0	0.0	0.0	19.7	19.7	18.9	17.7	15.3
22.7	22.3	23.4	22.1	21.6	20.2	19.7	19.9	19.6	19.2	18.9	17.6	16.9
22.0	22.6	22.0	22.4	21.6	21.5	20.7	20.5	20.4	20.2	19.4	18.2	17.3
21.9	21.5	22.7	22.4	21.2	21.7	20.9	20.4	20.3	20.0	20.0	19.0	17.8
22.2	21.7	22.5	21.3	20.6	21.4	21.1	19.4	19.4	19.7	19.1	18.6	18.3
22.4	21.4	22.2	21.5	21.0	20.5	21.0	20.5	20.3	20.1	19.7	19.2	18.7
22.7	21.5	21.5	21.7	21.9	20.5	20.7	20.7	20.6	20.7	20.0	19.8	18.5
23.3	21.8	21.9	21.4	22.2	2117	21.0	21.0	20.1	19.6	19.8	18.9	18.2
22.6	22.0	22.6	21.9	22.6	22.4	22.1	21.9	20.8	0.0	18.6	19.0	18.7
21.4	21.7	21.7	21.6	22.1	21.7	21.8	21.7	21.6	20.5	19.9	19.6	19.2
20.8	21.3	21.0	21.7	21.9	21.8	21.8	21.3	22.2	21.3	21.0	20.0	19.6

RESIDUAL STATISTICS
AVERAGE = 20.691, MINIMUM = 14.091 , MAXIMUM = 24.171
STANDARD DEVIATION = 1.7705 ; THE NUMBER OF OBSERVATIONS = 150.

TABLE IV(j) RESIDUALS BETWEEN SST(SMMR) AND SST(AVHRR OPERATIONAL)

RSIDSC (13.13): (AVERAGE = -21.545)

0.0	0.0	-23.0	-22.7	0.0	0.0	0.0	-20.8	0.0	0.0	-18.9	-18.1	-17.2
0.0	0.0	22.7	22.6	0.0	0.0	0.0	0.0	0.0	19.6	18.9	18.2	17.4
0.0	-22.8	-22.6	-22.3	-22.0	0.0	0.0	0.0	-20.2	-19.6	-19.0	-18.3	-17.6
-22.7	-22.6	-22.5	-22.2	-21.9	-21.6	-21.2	-20.8	-20.3	-19.7	-19.1	-18.5	-17.8
-22.6	-22.5	-22.4	-22.2	-21.9	-21.6	-21.3	-20.9	-20.4	-20.3	-19.7	-19.1	-18.4
-23.3	-23.3	-23.2	-23.0	-22.8	-22.5	-22.2	-21.8	-21.4	-20.9	-20.3	-19.8	-19.1
-23.3	-23.3	-23.2	-23.1	-22.9	-22.6	-22.3	-22.0	-21.6	-21.1	-20.6	-20.1	-19.4
-23.3	-23.3	-23.3	-23.2	-23.0	-22.8	-22.5	-22.2	-21.9	-21.4	-21.0	-20.4	-19.8
-23.4	-23.4	-23.4	-23.3	-23.2	-23.0	-22.8	-22.5	-22.2	-21.8	-21.3	-20.1	-19.3
22.0	22.0	22.1	22.0	21.9	21.8	21.6	21.3	21.0	20.7	21.1	20.6	20.1
-22.1	-22.2	-22.3	-22.3	-22.2	-22.1	-21.9	-21.7	-21.4	0.0	-20.7	-20.3	-20.6
-22.3	-22.5	-22.6	-22.6	-22.6	-22.5	-22.3	-22.2	-21.9	-21.6	-21.3	-20.9	-20.4
-22.7	-22.9	-23.0	-23.0	-23.0	-23.0	-22.9	-22.7	-22.5	-22.3	-21.9	-21.6	-21.1

RESIDUAL STATISTICS:

AVERAGE = -21.454 , MINIMUM = -23.392 , MAXIMUM = -17.229

STANDARD DEVIATION = 1.4679 ; THE NUMBER OF OBSERVATIONS = 150.

least 15 degrees low. This discrepancy in the SMMR data corresponds with the amount of bias in the SMMR cell tape data which others have noted.

Table V shows the average results for all seven 780 x 780 km SMMR blocks. The average of the average residuals is -.149, and the average standard deviation is 1.022. It may be seen that most values derived from the AVHRR and SMMR data coincide reasonably well with the NOAA operational product tape data.

TABLE V: FINAL RESULTS

Block Number	Date (1979)	Center Latitude	Center Longitude	Ave. Water Vapor(gm/cm^2)	Ave. Uncorrected T_A (^oK)	Ave. Trial T_s(^oK)	Ave. Final T_s(SST_A)(^oK)	Ave. Operational SST(SST_O)(^oK)	Ave. Residual (^oK)	Max. Residual (^oK)	Min. Residual (^oK)	of Residual (^oK)
(1)	Feb 27	26.9°S	18.9°W	3.349	291.80	296.09	296.16	297.01	- .854	1.617	- 3.138	.874
(2)	Feb 15	4.2°S	126.7°W	5.036	294.54	299.56	299.63	299.14	.486	1.836	- 2.031	.885
(3)	Feb 27	3.1°S	129.4°W	4.692	291.75	300.36	299.01	300.01	1.493	3.819	- .407	1.041
(4)	Feb 25	29.9°N	50.6°W	2.230	288.60	290.51	290.54	292.58	-2.043	.126	- 5.174	1.008
(5)	Feb 15	23.6°S	17.7°W	3.426	295.41	298.38	298.43	298.35	.077	2.394	- .847	.453
(6)	Feb 25	2.0°S	120.6°W	4.687	294.13	298.65	298.73	298.13	.604	1.999	- 2.476	.815
(7)	Feb 27	25.0°S	84.4°E	3.782	291.17	296.58	296.66	297.47	- .808	2.072	-12.165	2.078

Average of average residuals = 149°K

Average of standard deviation of residual = 102°K

5.0 CONCLUSIONS

In this study, microwave measurements from the Nimbus-7 SMMR were used to derive the atmospheric precipitable water, which was then used to obtain the atmospheric correction for use with AVHRR thermal IR measurements to obtain sea surface temperature. The resulting SST's compared were with the NOAA operational sea surface temperature measurements, and the two sets of measurements were found to be in reasonable agreement. For the limited sample analyzed in this study the average residuals between the two sets of measurements was .15°K with the NOAA operational SST's being slightly greater.

This demonstrates that the use of microwave measurements is a promising tool for correcting IR sea surface temperatures for water vapor effects even under cloudy conditions. This can be done either by using Nimbus-7 SMMR and TIROS-N or NOAA-6 or NOAA-7 AVHRR measurements and matching them, or by using instruments from any future satellites where both the scanning IR and microwave instruments are on board. To further check the accuracy of this algorithm, the results from it should be compared with actual surface truth such as that from buoys. Also, since the method of cloud thresholding "by hand" used in this study is impractical for operational use, the effects on this algorithm of automating the cloud thresholding procedure should be studied.